Article

Spatio-temporal Features of Urban Heat Island and its Relationship with Land Use/Cover in Mountainous City: A Case Study in Chongqing

Chunxia Liu[1,2,3] and Yuechen Li[1,2,3,*]

[1] College of Geography and Tourism, Chongqing Normal University, 37 Daxuechengzhong Road, Chongqing 401331,China;liuchunxia_2004@163.com
[2] Chongqing Key Laboratory of GIS Application, 37 Daxuechengzhong Road, Chongqing 401331,China; liyuechen@cqnu.edu.cn
[3] Institute of Eco-environment remote sensing in Three Gorges Reservoir Region, Chongqing Normal University, 37 Daxuechengzhong Road,Chongqing 401331,China; liyuechen@cqnu.edu.cn
* Correspondence: liyuechen@cqnu.edu.cn; Tel.: +86-23-6536-2776

Abstract: The urban heat island (UHI) becomes more and more serious with the acceleration of urbanization. Many researchers have shown interest in studying the UHI by using remote sensing data. But these studies rarely examine the mountainous cities. The studies on UHI in mountainous cities often used empirical parameters to estimate the land surface temperature (LST), and lacked satellite-ground synchronous experiment to test the accuracy. This paper revised the parameters in mono-window algorithm used to retrieve the LST according to the characteristics of mountainous cities. This study examined the spatial and temporal patterns of the UHI intensity in Chongqing, a typical mountainous city, and its relationship with land cover from 2007 to 2011 based on the Landsat TM data and the improved method. The accuracy of the LST derivation increased by about 1°C compared to the traditional method. The high LST areas increased and extended from the downtown to suburban area each year, but the rate of change decreased. The UHI is dramatically impacted by the rivers. There is a good relationship between the urban sprawl and the UHI. The LST was reduced by about 1°C within a 300m distance from large urban fringe green spaces. The urban landscape parks had a strong effect relieving the UHI at a 100m distance. The LST was reduced by about 0.5°C. The study greatly improves the accuracy of LST derivation, and provides a reliable parameters for the UHI researched in mountainous city.

Keywords: spatio-temporal pattern; land cover; mountainous city; Chongqing

1. Introduction

Urbanization is one important attribute of regional social and economic development. At the same time, the eco-environment problems caused by urban heat island (UHI) become more and more serious with the acceleration of urbanization [1,2]. In recent decades, many researchers have shown interest in estimating the magnitude of UHI, analyzing its spatio-temporal evolution features, understanding its implication with respect to a broad set of environmental factors, and looking for the measures to reduce its detrimental effects [3-10]. The studies on the UHI phenomenon can be divided into two types: ground based observed air temperature in urban and rural weather stations and Remotely-sensed data based land surface temperature [11]. It is well known that the air temperature defined UHI can be used to analyze the long term trend, but considerable efforts must be made to correct air temperature biases when comparing UHI effects across different regions. It is difficult to analyze the UHI phenomenon in the regions where there are no enough weather stations. The remote sensing data with the advantages of large area, synchronization, and spatial coverage has become the effective data for studying UHI phenomenon [12-15]. Among many UHI algorithms based on remote sensing, the mono-window algorithm,

because it is easy and feasible, is widely used in the studies of UHI[3,9,15-18]. While these detailed studies provide an excellent basis for understanding UHI, there are also some limitations: (1) These studies rarely examined the mountainous cities; (2) Few studies on UHI in mountainous cities based on remote sensing data often used empirical parameters to estimate the land surface temperature (LST). It is therefore hampered by the lack of proper parameters to retrieve the LST in mountainous cities. (3) Many studies lacked satellite-ground synchronous experiment to test the accuracy.

Chongqing, a typical mountainous city, is located at the valley between Mount Tongluo and Mount Zhongliang. The eco-environmental problems caused by UHI are becoming increasingly acute with the acceleration of urbanization. Ren found that the UHI intensity of Chongqing increased year by year. The UHI effect was stronger in winter and at night [19]. Li et al. indicated that the UHI was contemporaneous with the Urban Wet Island (UWI) in Chongqing. The vertical structure of UHI was shown as the city being covered by warm moist air at 200-300m above the river level [20]. He et al. discovered that the UHI was influenced by the mountainous terrain features and city layout in Chongqing [21]. Dan et al. thought that the Yangtze River and Jialing River had important effects on the UHI of Chongqing [22]. Some other scholars also did some research on UHI in Chongqing [23, 24]. Although Chongqing's UHI effect has been well studied, most of the literature is based on weather station data, which neglects the spatial extension and distribution of UHI. These studies also lack necessary verification of their precision. Furthermore, it is necessary to better understand how the impact factors, especially urban green spaces, influence the UHI effect in Chongqing.

In this study we rectify the parameters used in the mono- window algorithm according to the terrain features of Chongqing. We use a combination of Landsat TM data, automatic weather station data, and satellite-ground synchronous experiment data to estimate the LST, test its accuracy, and examine the relationship between the impact factors and the UHI variations in Chongqing. The main objective of this study is to provide a suitable quantitative method to study UHI in mountainous cities.

2. Materials and Methods

2.1. Study area

Chongqing municipality, one of the fastest developing cities in China over the past twenty years, is situated in southwest China. Characterized by rugged hills, Chongqing is a typical mountainous city and is also one of the three famous "stoves" of China. The study area is located between 106°23'2.4"E-106°41'45.6"E and 29°20'31.2"N-29°43'26.4"N in the southwest of Chongqing municipality, with a total area of approximately 780km^2 (Figure 1). It has a humid subtropical monsoon climate, and receives an average annual precipitation of 1000mm. The average annual temperature is 18.4 ºC. The Yangtze River and Jialing River go through the area roughly from south to north and from west to east respectively, uniting in the city center. Separated by the terrain and the rivers, naturally, the study area forms a multi-center structure. The UHI phenomenon in the study area is obvious because of the air circulation caused by the terrain barrier, and the high population and building density caused by rapid urbanization [25].

2.2. Data and image pro-processing

Satellite remote sensing offers a great opportunity to acquire continuous LST data without direct physical contact with the surface, with sufficient spatial resolution to distinguish between urban and surrounding rural areas [26]. The Landsat TM is one of the most widely used remote sensing data for UHI studies. Five Landsat TM images (i.e., Sept 20, 2007; Jul. 20, 2008; Sept. 24, 2009; Aug. 11, 2010 and Aug. 30, 2011) were used for retrieval of LST in this study. The data acquisition dates had highly clear atmospheric conditions, and the images were acquired from the Institute of Remote Sensing and Digital Earth Chinese Academic of Sciences Data Center, which corrected the radiometric and geometrical distortions of the images before delivery. The Landsat images were further rectified to a common Universal Transverse Mercator coordinate system based on 1:10,000

scale topographic maps, and were resampled using the nearest neighbor algorithm with a pixel size of 30 by 30 m for all bands, including the thermal band. The resultant RMSE was found to be less than 0.5 pixels. In addition, the meteorological data from 4 standard weather stations, 11 intensive automatic weather stations, and 19 field observing sites, the urban planning data, the land use/cover, and some other auxiliary data were used to assist in the analysis.

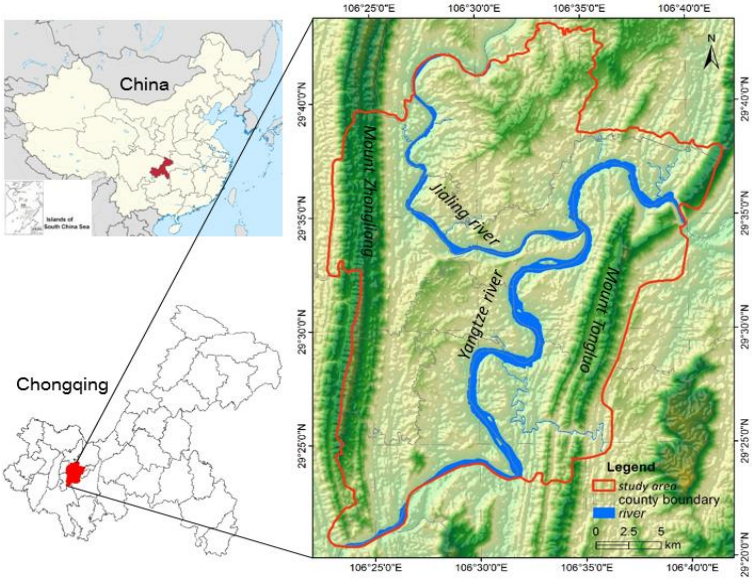

Figure 1. A map of the study area.

The sensor TM band 6 on Landsat 5 measures the radiances at the top of the atmosphere, and its brightness temperatures can be derived using Plank's law [27]. The approach to the retrieval of temperature was described in the Landsat 5 User's Handbook. The following equation was used to convert the digital number (DN) of Landsat TM TIR band into spectral radiance:

$$L_\lambda = \mathrm{DN}\ (L_{max} - L_{min})\ /255 + L_{min}, \quad (1)$$

Where, $L_\lambda$is spectral radiance; DN represents the digital number of band 6; L_{max}=1.56mWcm^{-2}sr^{-1}um^{-1}andL_{min}=0.1238mWcm^{-2}sr^{-1}um^{-1}(given in the header files of the images) are the maximum and minimum spectral radiance of band 6 respectively.

The next step is to convert the spectral radiance to at-satellite brightness temperature under the assumption of uniform emissivity. The conversion formula is:

$$T_6 = K_2/\ln(1 + K_1/L_\lambda), \quad (2)$$

Where, T_6 is the effective at-satellite brightness temperature in K of band 6; L_λ is spectral radiance; K_1=60.776mWcm^{-2}sr^{-1}um^{-1} and K_2=1260.56 K are pre-launch calibration constants.

2.3. Derivation of LST and improvement of the parameters

The methods for the retrieval of LST from satellite TIR data can be broadly classified into three categories: single-channel methods, multi-channel methods (split-window algorithm, SWA), and multi-angle methods [28-30]. In comparison with other methods, the mono-window algorithm is simpler and only three parameters (the average atmospheric operative temperature, land surface emissivity and atmospheric transmittance) are needed; therefore, the mono-window algorithm was used to calculate the LST for the Landsat TM images. The mono-window algorithm's calculation formula is as follows [31]:

$$T_s = \{a_6(1 - C_6 - D_6) + [b_6(1 - C_6 - D_6) + C_6 + D_6]T_6 + D_6T_a\}/C_6, \quad (3)$$

Where, T_s is the emissivity corrected land surface temperatures; a_6 and b_6 are regression coefficients. In most studies, the values of the a_6 and b_6 were given roughly as -67.35535, 0.458608, respectively, within the temperature range of 0~70 °C. The TM images used in this study are all at

noon in summer (approximately 11:17 am), and the range of temperature variation is small. In this case, the a_6 and b_6 are equal to -67.9542 and 0.45987, respectively (within the temperature range of 20~50°C); $C_6=\tau_6\varepsilon_6$ and $D_6=(1-\tau_6)[1+\tau_6(1-\varepsilon_6)]$ are the intermediate variables; τ_6 is the atmospheric transmittance; ε_6 is the land surface emissivity; T_6 is the effective at-satellite brightness temperature of band 6; and T_a is the effective mean atmospheric temperature.

τ_6, ε_6 and T_a are three essential parameters in the mono-window algorithm. Many researchers used these empirical values in their studies. But, in fact, the mono-window algorithm is sensitive to parameters. So it is obvious that the empirical values are not suitable to the retrieval of LST in Chongqing, a typical mountainous city with complex terrain features. In this study we improved the method to estimate the three essential parameters, and the retrieval accuracy of LST was also improved.

2.3.1. Determination of the land surface emissivity (ε_6)

The urban area can be divided into water, natural surface, and built-up. If land over is water then ε_w= 0.995. If land cover is natural surface and NDVI<0.05 then it is bare land, and ε_s= 0.972. If NDVI> 0.7, it is fully covered by vegetation, and ε_v =0.986.When NDVI ϵ[0.05,0.7], the land surface emissivity (ε_6) was computed as follows [32]:

$$\varepsilon_6 = P_v R_v\varepsilon_v + (1- P_v) R_s \varepsilon_s + d_\varepsilon, \quad (4)$$

When land cover is built-up, the land surface emissivity (ε_6) was computed as following follows [32]:

$$\varepsilon_6 = P_v R_v\varepsilon_v + (1- P_v) R_m \varepsilon_m + d_\varepsilon, \quad (5)$$

Where, P_v is vegetation coverage; R_v =0.9332+0.0585P_v is vegetation temperature ratio; ε_v =0.986 is land surface emissivity with very high vegetation coverage; R_m =0.9886+0.1287P_v is the building surface temperature ratio; ε_m =0.972 is the building surface emissivity. The effect of d_ε is negligible in many studies. They all assume that the land surface is flat. As mentioned before, the terrain of Chongqing is complex. In this paper, we estimated the value of d_ε according to the vegetation coverage (when $P_v\leq0.05$, d_ε=0.0038; when $P_v>0.05$, d_ε=0.0038(1- P_v)).

2.3.2. Determination of atmospheric transmittance (τ_6)

The atmospheric transmittance (τ_6) can be estimated by the following equation [31]:

$$\tau_6 = 0.97429-0.08007\omega, \quad \omega\epsilon[0.4,1.6];\tau_6 = 1.031412-0.11536\omega, \quad \omega\epsilon[1.6,3.0], \quad (6)$$

Where, ω is atmospheric water vapor content in g·cm^{-2}. In many studies ω was often estimated by experience. In our study we calculate it as follows [33]:

$$\omega = a_0+ a_1e, \quad (7)$$

Where, a_0 and a_1 are empirical constants. The central latitude and average altitude of the study area are 29.5° and 350m respectively, so we can determine ω = 0.04691+ 0.19604e, according to Yang *et al*. e is absolute vapor pressure. It can be calculated as follows [33]:

$$e = 0.6108\exp[17.27(T_0-273.15)/(237.3 + T_0 -273.15)]RH, \quad (8)$$

Where, T_0 is air temperature; RH is relative humidity. Due to a lack of meteorological data, most of the studies use the meteorological data from standard weather stations to estimate e. Unfortunately, urban areas often have few weather, making the accuracy of e unsatisfactory. In this study the meteorological data from 4 standard weather stations, 11 intensive automatic weather stations, and 19 field observing sites are combined to determine the value of e. We therefore generated satisfactory results.

2.3.3. Determination of effective mean atmospheric temperature (T_a)

According to Qin et al., for mid-latitude summer T_a can be approximated as [31]:

$$T_a = 16.011+0.92621\ T_0, \quad (9)$$

Where, T_0 is near-surface air temperature. In this paper, we improved the accuracy of T_a by using the integrated meteorological data from standard weather stations, intensive automatic weather stations and field observing sites.

3. Results

3.1. Retrieval Accuracy validation of LST based on satellite-ground synchronous experiment

The best way to validate retrieval accuracy is to compare the in situ ground truth measurements of LST with the retrieved ones from the Landsat TM data of a specific region. On Aug. 30, 2011, we carried out a satellite-ground synchronous experiment at a Landsat TM pass over the study area. We recorded the air temperature, LST, wind speed, and air humidity at 46 field sites each 15 minutes from 9:30 am to 3 pm. In actual operation, we used the data from 19 sites with high reliability to validate the retrieval accuracy of LST (Table 1).

Table 1. Retrieval accuracy validation of LST based on satellite-ground synchronous experiment.

Sites	Land use/cover	Ground measurement LST T_{true} (°C)	Method of improved parameters		Method of empirical parameters	
			Retrieved LST T_{s1} (°C)	Absolute difference $\lvert T_{true} - T_{s1} \rvert$ (°C)	Retrieved LST T_{s2} (°C)	Absolute difference $\lvert T_{true} - T_{s2} \rvert$ (°C)
Bailin	Grassland	31.00	33.06	2.06	31.05	0.05
Guanyinqiao	Shrub	39.90	39.27	0.63	35.93	3.97
Longtousi	Square	37.20	36.92	0.28	33.57	3.63
Yuanyuang	Farmland	35.20	37.15	1.95	34.82	0.38
Houbao	Residential area	35.10	35.71	0.61	32.58	2.52
Caiyuanba	Square	42.50	39.84	2.66	37.42	5.08
Nanshan	Wood	36.00	35.83	0.17	31.95	4.05
Zhaomushan	Wood	26.50	29.20	2.70	27.69	1.19
Jinyuan	Pavement	27.00	30.00	3.00	26.14	0.86
Dachuan	Square	43.20	38.98	4.22	36.95	6.25
Shaping	Wood	34.00	34.20	0.20	30.47	3.53
Huahui	Wood	37.70	34.10	3.60	32.98	4.72
Jialing river1	River beach	29.10	30.57	1.47	26.16	2.94
Jialing river2	Water	28.50	30.57	2.07	32.57	4.07
Dadukou	Wasteland	36.50	38.56	2.06	34.90	1.60
Chaotianmen	Grassland	36.00	36.85	0.85	33.09	2.91
Pingtingshan	Wood	31.00	33.33	2.33	29.02	1.98
Yangtze river1	River beach	27.00	28.77	1.77	28.72	1.72
Yangtze river2	Water	26.00	28.77	2.77	26.5	0.50
Mean	-	33.65	34.30	1.86	31.71	2.73

Peer-reviewed version available at Sustainability 2018, 10, 1943; doi:10.3390/su10061943

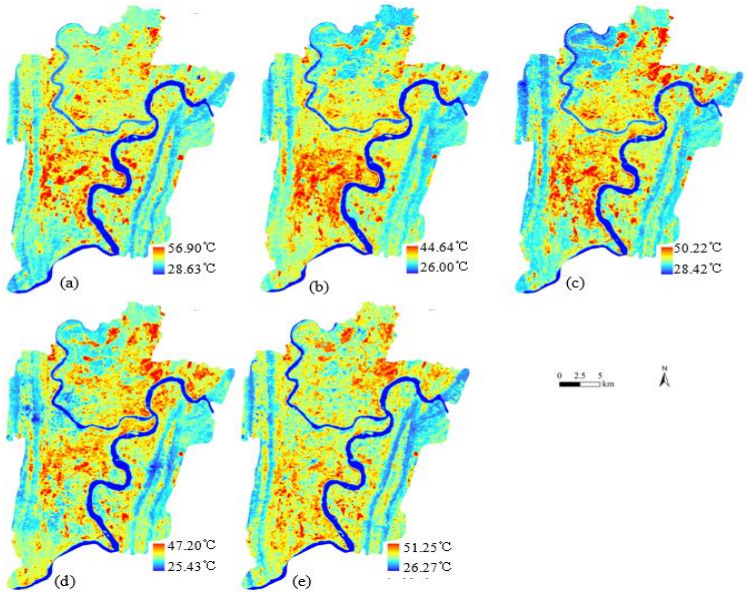

Figure 2. Land surface temperature distribution maps: (**a**) Sept 20, 2007; (**b**) Jul. 20, 2008; (**c**) Sept. 24, 2009; (**d**) Aug. 11, 2010; (**e**) Aug. 30, 2011.

The results in Table 1 indicate that the LSTs retrieved after improving the parameters are generally higher than the in situ ground truth measurements of LSTs. The mean values are 34.30°C and 33.65°C respectively with a difference of 0.65°C. The maximum, minimum, and mean absolute difference between T_{true} and T_{s1} are 4.22°C, 0.17°C and 1.86°C. We also compared the retrieved LST by comparing the empirical parameters with the ground truth LST. The former are generally lower than the latter. The mean value is lower by 1.94°C. The maximum, minimum, and mean absolute difference between T_{true} and T_{s2} are5.08°C, 0.05°C and 2.73°C. The experimental results also show that the LSTs retrieved by using the improved parameters are more accurate compared to the LSTs retrieved based on the previous parameters. This good matching of the LSTs retrieved to the actual ones confirms the applicability of the improved parameters to the UHI studies in mountainous cities.

LST images from five periods Landsat TM6 data of the study area were calculated using the improved parameters mono-window algorithm (Figure 2, Table 2). In order to eliminate the effects of the environmental factors, we normalized the LSTs to 0~1, and divided them to seven levels (i.e., very high temperature area, high temperature area, sub-high temperature area, medium temperature area, sub-medium temperature area, low temperature area, and very low temperature area) by using the natural breaks grading method (Figure 3, Table 3).

3.2. Spatio-temporal features of UHI

The temporal variation and spatial distribution of annual UHI over the study area are shown in Figure 2, Figure 3, Table 2, and Table 3. The results suggest that The LSTs show a gradually increasing trend from 2007 to 2011, and that the spatial pattern of the UHI changed from a scattered pattern in 2007 to a more contiguous pattern in 2011, along with the expansion of the regional urban system. The centers of high temperature were consistent with built-up and bare land areas and the low-temperature centers are located in the area of two rivers (i.e., Yangtze River and Jialing River) and two mountains area (i.e., Mount Zhongliang and Mount Tongluo). The relatively high temperature areas (i.e. very high LST area and high LST area) shifted from south to north and expand from the central city to the outskirts. On August 20, 2011, the mean LST was 37°C. In most of the study area, the LST was above 35°C and the maximum LST was even up to 51.26°C. Compared to 2007, the mean LST increased by 0.29°C, the distribution of the relatively high temperature areas became more even. The distribution of high-temperature centers was more disperse, and their inner structure and composition obviously changed. These distributions and changes of the UHI effect are closely related to the types and functions of the different underlying surface and their changes.

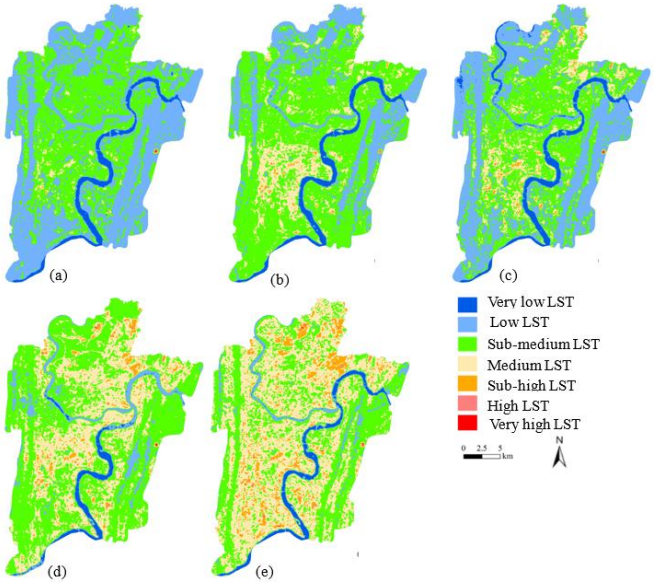

Figure 3. Land surface temperature levels maps: (**a**) Sept 20, 2007; (**b**) Jul. 20, 2008; (**c**) Sept. 24, 2009; (**d**) Aug. 11, 2010; (**e**) Aug. 30, 2011.

In the study area, the very low LST areas were mainly the large water bodies, such as ponds, reservoirs and rivers, and changed with the water level. There were few changes from 2007 to 2009, but the area and area ratio obviously decreased (Table 2). The low LST areas concentrated on the high vegetation coverage areas and some small water bodies. After 2009, the area sharply decreased. The sub-medium LST areas were located in the sub-high vegetation coverage areas and farmlands. They changed in volatility from 2007 to 2011. The medium LST areas were the forests and grasslands with low vegetation coverage and some farmlands, and increased rapidly over time, from 15.29km^2 in 2007 to 250.18km^2 in 2011. The high LST areas, and very high LST areas mainly distributed in the industry lands, built-up areas, and development and construction areas. Compared to 2007, the total area and ratio of the two types quickly increased as a general trend and were up to 2.35km^2 and 0.30%, 1.31km^2 and 0.17% respectively in 2010 and 2011. The relatively high temperature areas were spotty and distributed linearly in 2007, and the large high temperature areas were mainly located in the business and industry concentrating areas, such as Yuzhong, Dadukou and Jiulongpo, etc. In 2008, the relatively high temperature areas also distributed in the business and industry centers within the inner ring road, but the spatial structure gradually transformed from a dispersedly spotty and linear distribution to continuous area distribution. At the same time, many constructing areas became the new high temperature centers. In 2009, when the lands within the inner ring road had not met the urban development, some new high temperature areas appeared outside inner ring road, such as Lianglu, Jingkou, Tangjiatuo, Lishuwan, Chonggang, Changgang, etc. The LST was generally higher in 2010. The main change in this year was the obviously northward shift of the high-temperature centers, and the expansion of the relatively high temperature areas (from 0.76km^2 in 2009 to 57.07km^2 in 2010). In 2011, the relatively high temperature areas decreased compared to 2010 (from 2.35 km^2 in 2010 to 1.31 km^2 in 2011), but it was still far more than it was in 2007, 2008 and 2009. Although the relatively high LST areas were largest in 2010, apparently there was a general trend of increasing UHI effect from 2007 to 2011.

Table 2. LSTs of the five dates. (°C)

Date	LST_{min}	LST_{max}	LST_{mean}	LST_{std}
2007-9-20	28.63	56.90	36.71	2.02
2008-7-20	26.00	44.64	33.24	2.02
2009-8-24	28.43	50.22	35.04	2.25
2010-8-11	25.44	47.20	34.01	2.24
2011-8-30	26.28	51.26	37.00	2.78

Table 3. The area of different LST levels from 2007 to 2011.

Level	Area of 2007 (km²)	Area ratio (%)	Area of 2008 (km²)	Area ratio (%)	Area of 2009 (km²)	Area ratio (%)	Area of 2010 (km²)	Area ratio (%)	Area of 2011 (km²)	Area ratio (%)
Very low LST	33.20	4.26	33.71	4.32	39.29	5.04	26.88	3.45	20.38	2.61
Low LST	385.46	49.42	180.73	23.17	323.25	41.44	36.29	4.65	56.38	7.23
Sub-medium LST	345.85	44.34	466.31	59.78	332.65	42.65	288.78	7.02	429.43	35.06
Medium LST	15.29	1.96	95.44	12.24	78.18	10.02	371.79	47.67	250.18	32.07
Sub-high LST	0.89	0.11	4.27	0.55	6.71	0.86	54.72	7.02	23.13	2.97
High LST	0.14	0.02	0.35	0.04	0.67	0.09	2.17	0.28	1.22	0.16
Very high LST	0.07	0.01	0.00	0.00	0.09	0.01	0.18	0.02	0.09	0.01
Sum of high and very high LST	0.21	0.03	0.35	0.04	0.76	0.10	2.35	0.30	1.31	0.17

3.3. Relationship between LST and NDVI

The Normalized Difference Vegetation Index (NDVI) was calculated for each image. The negative correlations were found between NDVI and LST by comparing both images. In order to further study their quantitative relationship, the NDVI and LST images on August 30, 2011 are selected as samples to establish the linear regression. Its regression equation was given as follows.

$$LST = -6.212NDVI + 38.89 \quad (NDVI \geq 0), \tag{10}$$

With the increasing of NDVI, the LST decreased from approximately 45°C to 33°C. When NDVI was approximately 0.18, some pixels had a higher LST. After analyzing the NDVI, LST and high resolution images, we find that most of these pixels were in the new construction areas.

3.4. Relationship between UHI and urban expansion

In the paper, the LST changes were detected from 2007 to 2011, and the amplitude of changes are classified on Table 4, Figure 4.

Table 4. Classification standard of the LST change.

Types	Strong LST decrease	Slight LST decrease	No chang	Slight LST increase	Strong LST increase
$LST_{2011} - LST_{2007}$	＜-3°C	-3-1°C	-1-1°C	1-3°C	＞3°C

In Figure 4 we find that the LST decrease areas are mainly the water bodies and high vegetation coverage areas, the no-change areas are distributed in the old urban districts, and the LST increase areas are located at the north and south of the study area. From 2007 to 2011 the urban area also mainly expanded to north and south (Figure 4-b). By comparing Figure 4-a with Figure 4-b, there is a good correlation between the expansion of urban area and UHI in pattern, position and amount. The urban area expanded by 85.9km² during the five years and the strong LST increase areas showed a rise of 54.57km² during the same time. It is obvious that the urban expansion was the main contributor to the UHI.

Peer-reviewed version available at Sustainability 2018, 10, 1943; doi:10.3390/su10061943

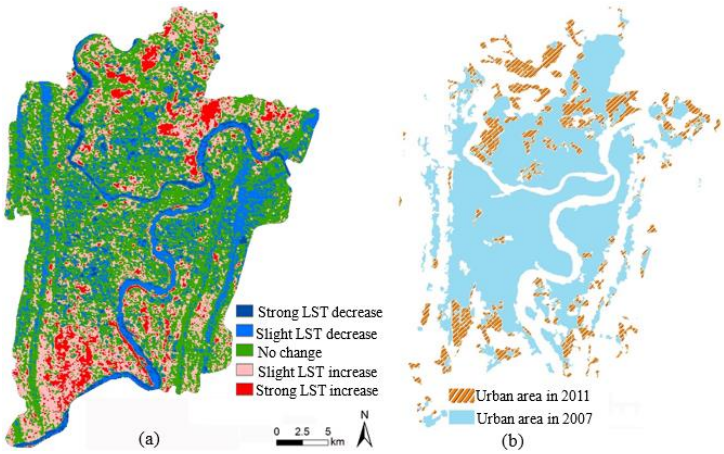

Figure 4. Relationship between UHI and urban expansion: (**a**)LST change map from 2007 to 2011; (**b**) urban expansion map form 2007 to 2011.

3.5. Relationship between UHI and land use/cover

In this paper, we also explored the effect of different land use/cover types for UHI in a mountainous city. Five land use/cover types were classified in the study area (i.e. built-up, bare land, vegetation, water and road). Vegetation is the area containing forests, shrubs, grasslands and crops. Water includes reservoirs, ponds and rivers. The area under development is similar to bare land. The map of land use/cover was retrieved from a Landsat TM image on Aug. 30, 2011. To study the temperature relationship of different land use/cover types, the maximum, minimum and mean LST of different land use/cover types were derived by averaging all corresponding pixel values (Table 5). It can be found from Table 5 that the maximum and mean LST in bare land are all highest (47.20°C and 36.91°C) followed by built-up (46,78°C and 35.24°C), and the maximum and mean LST in water are lowest due to its high heat capacity.

To further study the relationship between LST and land use/cover types, the area of each LST level in different land use/cover types in 2011 was calculated (Table 6). Using the information, how the land use/cover types may have contributed to UHI can be estimated. From our analysis, it can be seen that almost all land use/cover types except water were distributed over the medium and sub-medium LST areas. The difference is that the areas of built-up, bare land and road located in medium LST areas were larger than those in sub-medium LST areas, but the vegetation was the opposite. The vegetation areas mainly showed the characteristics of low and very low LST. The relatively high LST areas concentrated in the built-up (14.11km^2) and bare land (8.95km^2). They nearly matched the total contribution. Most of the areas of built-up were medium and sub-medium LST. However, the low and very low LST areas were highly concentrated in water and vegetation. Both of them contributed more than 92% (70.93km^2) to the total area of low and very low LST areas in the study area. So it is easy to conclude that water and high coverage vegetation areas play an important role mitigating the UHI effect.

Table 5. LST in different land use/cover types in 2011.

Land use/cover	Minimum LST（°C）	Maximum LST（°C）	Mean LST（°C）
Buit-up	26.75	46.78	35.24
Bare land	28.72	47.20	36.91
vegetation	28.33	40.99	33.43
water	25.44	36.25	29.61
road	32.81	43.49	34.82

Table 6. Area of each LST level in different land use/cover types in 2011 (km^2).

Land use/cover	LST levels						
	Very low LST	Low LST	Sub-medium LST	Medium LST	Sub-high LST	High LST	Very high LST
Built-up	0.18	5.20	119.63	171.27	13.80	0.30	0.01
Bare land	0.00	0.34	4.87	19.65	8.05	0.82	0.08
Vegetation	0.01	24.48	293.80	56.89	1.02	0.02	0.00
Water	20.18	26.27	9.96	1.14	0.17	0.08	0.00
Road	0.00	0.00	0.10	0.18	0.00	0.00	0.00

3.6. Mitigating effects of different urban green spaces on UHI

Two types of urban green spaces (i.e. urban fringe forests and urban parks) were selected in the study. The urban fringe forests with large areas were retrieved from Landsat TM on Aug. 30, 2011(Figure 5), and the urban parks data was provided by Chongqing Park Management and Landscape Planning Bureau. The urban fringe forests include three primary parts: Mount Tongluo located in the east, Mount Zhongliang located in the west and some hills located in the north. Nine urban parks were selected as samples in the paper (i.e. Bolin park, Dongbu park, Eling park, Huahui park, Zhongyang park, Pingdingshan park, Shaping park, Shanhu park, Shimen park). We created six buffers per 50m for each urban fringe forest and urban park in this study, and estimated the mitigating effects of these urban green spaces on UHI (Table 7 and Table 8).

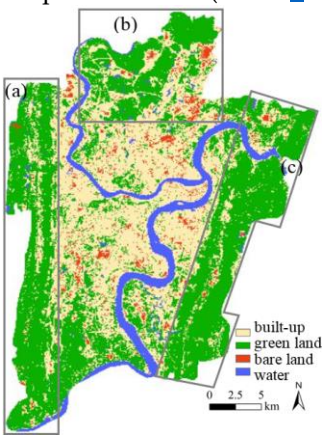

Figure 5. The green spaces map in 2011 : (**a**) west urban fringe forests; (**b**) north urban fringe forests; (**c**) east urban fringe forests.

From Table 7 and Table 8, it can be seen that there are obvious mitigating effects of the urban green spaces on UHI, but the mitigating effects decreased over distance. The urban fringe forests can achieve better performance than urban parks in mitigating UHI effects. For urban fringe forests, the two mountains (Mount Zhongliang in the west and Mount Tongluo in the east) showed a similar trend because of their similar features in area and spatial distribution. The decrease of LST changed from 1.85°C and 1.93°C to 1.47°C and 1.32°C, respectively, from the first buffer to the sixth buffer. The LSTs of buffers in the north showed a fast decline over distance, from 2.01°C to 0.53°C within 200m. This may be caused by the small area and different spatial pattern of the north urban fringe forest. In general, the urban fringe forests contributed to the decrease of LST by more than 1°C within 300m. The mitigating effects of the shorter distance to the forests the mitigating effects on UHI are more obvious.

Table 7. Mitigating effects of the urban fringe forests on UHI (°C).

Buffer (m)	Decrease of LST in west	Decrease of LST in north	Decrease of LST in east	Mean

0-50	1.85	2.01	1.93	1.93
50-100	1.81	1.36	1.76	1.64
100-150	1.65	0.86	1.59	1.37
150-200	1.58	0.53	1.56	1.22
200-250	1.58	0.37	1.49	1.15
250-300	1.47	0.22	1.32	1.00

[1] Decrease of LST = mean LST of buffer – mean LST of urban area.

Urban parks as the natural landscapes for citizens to rest can also, to some extent, play an important role in mitigating UHI effects. The differences between these parks, specifically the different areas and patterns to mitigated UHI effect (Table 8). In general, the LST in the first and second buffer of the parks, except Pingdingshan park, obviously decreased. The average contribution to the LST decrease in the first buffer (0-50m) was 0.51°C. The maximum and minimum decrease of LST were 1.73°C (Zhongyang park) and 0.06°C (Shaping park) respectively within the 0-50m distance. The parks had only slight effects on the LST when the distance exceeded 150m. So we should design and plan urban parks (area, pattern, location and quantity) scientifically and reasonably to maximize their effects on the UHI.

Table 8. Mitigating effects of the urban parks on UHI (°C).

Buffer (m)	Decreases of LST									Mean
	Bolin park	Dongbu park	Eling park	Huahui park	Zhongyang park	Pingdingshan park	Shaping park	Shanhu park	Shimen park	
0-50	0.83	0.29	0.37	0.15	1.73	0.33	0.06	0.43	0.44	0.51
50-100	0.29	0.30	0.31	-0.02	1.12	0.63	-0.27	0.30	0.11	0.31
100-150	-0.30	0.09	0.14	-0.04	0.33	0.83	-0.23	0.18	-0.11	0.10
150-200	-0.44	-0.10	-0.04	0.03	-0.43	0.75	0.02	-0.18	-0.12	-0.06
200-250	-0.22	-0.37	-0.29	0.00	-1.08	0.71	0.15	-0.45	-0.16	-0.19
250-300	-0.17	-0.22	-0.46	-0.12	-1.69	0.36	0.23	-0.25	-0.14	-0.27

[1] Decrease of LST = mean LST of buffer – mean LST of urban area.

4. Discussion

In this study we rectify the parameters used in the mono-window algorithm according to the characteristics of Chongqing, a typical mountainous city. We use a combination of Landsat TM data, automatic weather station data, and satellite-ground synchronous experiment data to estimate the LST, test its accuracy, and examine the relationship between the impact factors and the UHI variations in Chongqing. The accuracy of the LST derivation increased by about 1°C compared to the traditional method, and provides a reliable parameters for the UHI researched in mountainous city. Furthermore, all the analyses in this paper were based on the interpretation of remote sensing images, by which we analyzed not only the methods to retrieve the UHI, but also the phenomenon of UHI and its impact factors. The temporal and spatial variations of UHI were conducted by the analysis of multi-temporal remote sensing images. The remote sensing images are ideal for analyzing UHI, but it is difficult to select images with similar environmental conditions. In future study, several additional topics need to be explored. Firstly, the retrieval of UHI in mountainous cities is more complex than the cities on the plain. Although we have improved the method to estimate the three essential parameters, and the retrieval accuracy of LST was also improved, the retrieval method of LST needs to be improved to accommodate the complex terrain features and reduce the influence of inhomogeneous atmosphere condition in the mountainous cities. Secondly, although we have analyzed the effects of urban sprawl, LUCC and urban green spaces on the UHI, the impact mechanism of the shape, area, structure and distribution pattern of different land use/cover types in the urbanized area on UHI needs to be further studied. Thirdly, the effect of human activities and other impact factors on UHI must be investigated.

5. Conclusions

Chongqing is a typical mountainous city. In this paper, qualitative and quantitative analyses were used to study the spatio-temporal features of UHI and the relationship between LUCC and UHI in the study area. Several conclusions were drawn: (1) The accuracy of the LST derivation was improved by about 1°C compared to the traditional method. (2) The high LST areas increased and extended from the city center to suburban area each year, but the rate of change decreased. There were many minor changes inside high LST areas. (3) There were many rivers in the city and the UHI is dramatically impacted by the rivers. There is a good relationship between the urban expansion and the UHI. (4) The urban green spaces reduced the effects of UHI, but their functions decreased with the increase of distance from the green spaces. The large urban fringe green spaces composed a relative low temperature area and relieved the UHI in the large area. The LST was reduced by about 1°C within a 300m distance from the large urban fringe green spaces. The urban landscape parks had strong effects relieving the UHI at a 100m distance. The LST was reduce by about 0.5°C. The study greatly improves the accuracy of LST derivation, and provides a reliable parameters for the UHI researched in mountainous city.

Author Contributions: Yuechen Li and Chunxia Liu designed the paper. Chunxia Liu collected the data and wrote the paper. Yuechen Li revised the paper. All authors have read and approved the final manuscript.

Funding: This research was funded by the National Natural Science Foundation of China (41571419).

Acknowledgments: The authors wish to thank anonymous reviewers for their constructive comments and suggestions.

Conflicts of Interest: The authors declare no conflict of interest.

References

1. Wang, W.C.; Zeng, Z.M.; Thomas, R.K. Urban heat islands in China. Geophys. Res. Lett. 1990, 17, 2377-2380. [CrossRef]
2. Weng, Q.H.; Yang, S.H. Managing the adverse thermal effects of urban development in a densely populated Chinese city. J. Environ. Manage. 2004, 70, 145-156. [CrossRef]
3. Xu, M.; Qin, Z.H.; Zhu, Y. Spatial and temporal analysis of urban heat island in Suzhou City by remote sensing. Sci. Geogr. Sinica. 2009, 29, 529-534. (In Chinese) [CrossRef]
4. Priyadarsini, R.; Hien, W.K.; Wai David, C.K. Microclimatic modeling of the urban thermal environment of Singapore to mitgate urban heat island. Sol. Energy. 2008, 82, 727-745. [CrossRef]
5. Voogt, J.A.; Oke, T.R. Thermal remote sensing of urban climates. Remote Sens. Environ. 2003. 86, 370-384. [CrossRef]
6. Stathopoulou, M.; Cartalis, C. Daytime urban heat islands from Landsat ETM+ and Corine land cover data: An application to major cities in Greece. Sol. Energy. 2007, 81, 358-368. [CrossRef]
7. Streutker, D.R. Satellite-measured growth of the urban heat island of Houston, Texas. Remote Sens. Environ. 2003, 85, 282-289. [CrossRef]
8. Qian, L.X.; Ding, S.Y. Influence of land cover change on land surface temperature in Zhujiang Delta. Acta Geogr. Sinica. 2005, 60,761-770. (In Chinese) [CrossRef]
9. Zhao, S.Y.; Du, J.; Song, K.S.; Hu, X.L.A study on urban thermal field of Changchun city in summer based on satellite remote sensing. Sci. Geogr. Sinica. 2006, 26, 70-74. (In Chinese)[CrossRef]
10. Li, H.; Liu, Q.H.; Zou, J. Relationship of LST to NDBI and NDVI in Changsha-Zhuzhou-Xiangtan area based on MODIS data.. Sci. Geogr. Sinica. 2009, 29, 262-267. (In Chinese) [CrossRef]
11. Imhoff, M.L.; Zhang, P.; Wolfe, R.E.; Bounou, L. Remote sensing of the urban heat island effect across biomes in the continental USA. Remote Sens. Environ. 2010, 114, 504-513. [CrossRef]
12. Gallo, K.P.; McNab, A.L.; Karl, T.R.; Brown, J. F.; Hood, J. J.; Tarpley, J. D. The use of NOAA AVHRR data for assessment of the Urban Heat Island effect. J. Appl. Meteorol.1993, 32(5), 899-908. [CrossRef]
13. Weng, Q.; Dengsheng, L.; Jacquelyn, S. Estimation of land surface temperature–vegetation abundance relationship for urban heat island studies. Remote Sens. Environ. 2004, 89, 467-483. [CrossRef]
14. Gong, A.D.; Xu, J.; Zhao, J.; Li, J. A survey of study method for urban heat island. J. Nat. Disast. 2008, 17(6): 96-99. (In Chinese) [CrossRef]

15. Zhang, J.M.; Wang, P.L.; Ma, N.; Zhang, C. Spatial-temporal evolution of urban heat island effect in basin valley-a case study of Lanzhou city. Sci. Geogr. Sinica. 2012, 32(12): 1530-1537. (In Chinese) [CrossRef]
16. Qin, Z.H.; Zhang, M.H.; Aron; K.; Pedro; B. Mono-window algorithm for retrieving land surface temperature from Landsat TM6 data. Acta Geogr. Sinica. 2001, 56(4): 456-466. (In Chinese) [CrossRef]
17. Qiao, Z.; Tian, G.J. Spatiotemporal diversity and regionalization of the urban thermal environment in Beijing. J. Remote Sens. 2014, 18(3): 716-735. [CrossRef]
18. Jia; W.; Gao X.H. Analysis of urban heat island environment in a valley city for policy formulation: a case study of Xining city in Qinghai province of China. J. Geo-inf. Sci. 2014, 16(4): 592-601.
19. Ren; Q.F. The effects of urban heat island in the city of Chongqing. Chongqing Environ Sci. 1992, 14(3): 37-41.
20. Li; Z.H.; Tang, B.; Ren, Q.F. A study on the effects of the heat and wet island in the city of Chongqing during wintertime. Acta Geogr. Sinica. 1993, 48(4): 358-366.
21. He, Z.N.; Li, Y.H.; Chen, Z.J.; Gao, Y.H. Analysis on the urban heat island in summer of 2006 in Chongqing. J. Tro. Meteorol. 2008, 24(5): 527-532. (In Chinese) [CrossRef]
22. Dan, S.M.; An, H.F.; Ban, B.; Xu, H.X.; Yang, L.; Chen, G.Y. An analysis of urban heat island effects in Chongqing based on AVHR and DEM. Resour. Environ. Yangtze Basin. 2009, 18(7): 680-685. (In Chinese)
23. Liu, J.; Liu, X.Q.; He, Z.W. Urban heat island effect based on TM remote sensing image in Chongqing. Res. Soil Water Conserv. 2010, 17(5): 172-175. (In Chinese)
24. Yang, C.H.; Lei, B.; Wang, Y.C.; Zhang, S. Remote sensing of the spatial pattern of urban heat island effects and its influencing factors using TM data: a case study in core areas of Chongqing city. J. Basic Sci. Eng. 2014, 22(2): 227-238. (In Chinese)
25. Luo; X.B.; Peng, Y.D. Scale effects of the relationships between urban heat islands and impact factors based on a geographically-weighted regression model. Remote sens. 2016, 8, 760. [CrossRef]
26. Wang, C.Y.; Myint, S.W.; Wang, Z.H.; Song, J.Y. Spatio-temporal modeling of the urban heat island in the Phoenix metropolitan area: land use change implications. Remote sens. 2016, 8, 185. [CrossRef]
27. Dash, P.; Gottsche, F.M.; Olesen, F.S.; Fischer, H. Land surface temperature and emissivity estimation from passive sensor data: theory and practice-current trends. Int. J. Remote Sens. 2002, 23(13), 2563-2594. [CrossRef]
28. Zhang, Y.; Chen, L.Q.; Wang, Y.C.; Chen, L.G.; Yao, F.; Wu, P.Y.; Wang, B.Y.; Li, Y.Y.; Zhou, T.T.; Zhang, T. Research on the contribution of urban land surface moisture to the alleviation effect of urban land surface heat based on Landsat 8 data. Remote sens. 2015, 7, 10737-10762. [CrossRef]
29. Li, Z.L.; Tang, B.H.; Wu, H.; Ren, H.; Yan, G.; Wan, Z.; Trigo, I.F.; Sobrino, J.A. Satellite-derived land surface temperature: Current status and perspectives. Remote Sens. Environ. 2013, 131, 14-37. [CrossRef]
30. Jin, M.; Li, J.; Wang, J.; Shang, R. A practical split-window algorithm for retrieving land surface temperature from Landsat-8 data and a case study of an urban area in China. Remote Sens. 2015, 7, 4371-4390. [CrossRef]
31. Qin, Z.; Karnieli, A.; Berliner, P. A mono-window algorithm for retrieving land surface temperature from Landsat TM data and its application to the Israel-Egypt border region. Int. J. Remote Sens. 2001, 22(18), 3719-3764. [CrossRef]
32. Qin, Z.H.; Li, W.J.; Xu, B.; Chen, Z.X.; Liu, J. The estimation of land surface emissivity for Landsat TM6. Remote Sens. Land Resour. 2004, 61(3), 28-32. (In Chinese)
33. Yang, J.M.; Qiu, J.H. A method for estimating precipitable water and effective water vapor content from ground humidity parameters. Chinese J. Atmos. Sci. 2002, 26(1), 9-22. (In Chinese)